Surface Coating and Electrochemical Properties of $LiNi_{0.8}Co_{0.15}Al_{0.05}O_2$/ Polyaniline Composites as an Electrode for Li-ion Batteries

Young-Min Chung and Kwang-Sun Ryu*

*Department of Chemistry, University of Ulsan, Ulsan 680-749, Korea. *E-mail: ryuks@ulsan.ac.kr*
Received May 8, 2009, Accepted June 12, 2009

A new cathode material based on $LiNi_{0.8}Co_{0.15}Al_{0.05}O_2$ (LNCA)/polyaniline (Pani) composite was prepared by *in situ* self-stabilized dispersion polymerization in the presence of LNCA. The materials were characterized by fourier transform infrared spectroscopy (FT-IR), ultraviolet-visible spectroscopy (UV-Vis), X-ray diffraction (XRD), and scanning electron microscopy (SEM). Electrochemical properties including galvanostatic charge-discharge ability, cyclic voltammetry (CV), capacity, cycling performance, and AC impedance were measured. The synthesized LNCA/Pani had a similar particle size to LNCA and exhibited good electrochemical properties at a high C rate. Pani (the emeraldine salt form) interacts with metal-oxide particles to generate good connectivity. This material shows good reversibility for Li insertion in discharge cycles when used as the electrode of lithium ion batteries. Therefore, the Pani coating is beneficial for stabilizing the structure and reducing the resistance of the LNCA. In particular, the LNCA/Pani material has advantageous electrochemical properties.

Key Words: Lithium-ion battery, Cathode, Polyaniline, Lithium-nickel-cobalt-aluminum oxide, Conducting polymer

Introduction

Layered transition metal oxides have been extensively investigated as cathode materials for lithium ion batteries. Many transition metal oxides such as $LiCoO_2$ and $LiNiO_2$ have been developed as cathode materials for Li ion batteries.[1-3] Lithium nickel cobalt mixed oxide has played an important role in the field of lithium ion batteries.[4,5]

Ni can be used to improve the properties of $LiNi_{0.8}Co_{0.2}O_2$ and enhances its electrochemical properties.[6] However, $LiNi_{0.8}Co_{0.2}O_2$ has rapid moisture uptake and both Li_2CO_3 and LiOH impurities can be formed on the cathode surface,[7,8] which reduces its electrochemical performance. In recent years, many researchers have shown that the electrochemical characteristics of $LiNi_{0.8}Co_{0.2}O_2$ are closely related to the stability of the layered structure. Partial substitution by proper cations like Al ions are electrochemically inactive during the cycling process, and the strong Al–O bond can stabilize the layered structure. When Li ions participated in the intercalation-deintercalation, Al was inserted instead of Li ions in the hexagonal structure.[9,10]

To overcome the above problems, hybrid materials of $LiNi_{0.8}Co_{0.2}O_2$ combined with a classic conducting polymer such as Pani have been prepared.[11] The development of conducting composite has received significant attention, prompting new studies using other polymers combined at the molecular level with different inorganic solids.[12,13] There have also been satisfactory results using inorganic redox oxide, yielding systems suitable for electrochemical Li intercalation and their applicability as electrodes for rechargeable lithium batteries. Many of these systems involve inorganic hosts that exhibit a layered structure susceptible to exfoliation by guest polymer intercalation. Non-intercalable and three-dimensional structured metal oxides can also be combined with conducting polymers such as Pani or polypyrrole (Ppy) giving rise to microcomposites, materials combined at the micrometer scale, or even composites, taking into account the micrometer or nanometer scale size of the involved oxide particles.[14,15] The resulting cathodes can exhibit better electrochemical, mechanical, morphological, and thermal properties than the former components and some of them have also been tested in rechargeable lithium battery applications.[16]

Among the conducting polymers, Pani is particularly interesting due to its ease of doping, simple preparation, moderate conductivity, environmental stability, and low cost. In addition, Pani has wide applications in electronic, optical, and magnetic materials including formation, storage, rechargeable batteries, electrochromic display devices, sensors, and nonlinear optics.[17-19] In contrast to conventional homogeneous dispersion polymerization using an aqueous medium containing aniline, acid, and oxidant, this new polymerization is carried out in a heterogeneous biphasic (organic and aqueous) mixture without any stabilizers.

In this paper, we prepared a new cathode material based on LNCA/Pani by *in situ* self-stabilized dispersion polymerization in the presence of LNCA. The structure of LNCA/Pani and its electrochemical properties were studied by several techniques. The Pani coating improves the electrochemical cycling ability, capacity retention, and rate capability of LNCA/Pani composites.

Experimantal

Synthesis. The LNCA/Pani composite was prepared by *in situ* self-stabilized dispersion polymerization in the presence of LNCA (Ecopro Co. Ltd, Korea). The LNCA (20 g) was dispersed in ethanol/water (3:1 by volume) and then sonicated for 15 min using a Branson 3200 ultrasonic liquid processor

operating at 200 kHz. 0.98 mL (5 wt.%) aniline (reagent-grade; Aldrich) was added drop-wise to this dispersion, and the solution was sonicated for 10 min. Polymerization was carried out at 5 °C by drop-wise addition of ammonium peroxydisulfate [$(NH_4)_2S_2O_8$ or APS; Aldrich, aniline:APS at a 4:1 molar ratio] in 10 mL 1 M HCl with magnetic stirring for 15 h. The resulting solution was washed with absolute ethanol to remove monomer, oxidant, and its decomposition products, and then with acetone to eliminate low molecular weight organic intermediates and oligomers. The powder composite was vacuum dried at 60 °C. After drying, camphor sulfonic acid (HCSA; Aldrich) was used as a doping agent in acetone.

Characterization. Fourier transform infrared (FT-IR) spectra were recorded using a FT-IR spectrometer (Varian 2000) in the 500 ~ 3,000 cm^{-1} wave number range and the solid samples were diluted in KBr pellets. Ultraviolet-visible (UV-Vis) spectra were recorded by Varian Karry UV-Vis spectroscopy. The reagents were dissolved in NMP. Powder X-ray diffraction patterns were measured with a Rigaku ultra-X (CuK_a radiation, 40 kV, 120 mA) at a step scan rate of 0.02 °/s in the 2θ range of 10 ~ 80°. This was carried out to identify the crystalline phase of the as-prepared materials. The morphology and size of the powder particles were measured by scanning electron microscopy (SEM; Supra40) analysis.

The 2016R coin cells were assembled with LNCA/Pani, super-p, and polyvinylidene fluoride (PVDF; KF #1300) in N-methyl pyrrolidinone (NMP; Aldrich) solvent at a mass ratio of 92:4:4 (0.008 g/cm^2) as a cathode, Li metal as an anode, separator (Cellgard 2500), and the 1.3 M $LiPF_6$ solution dissolved in a 3:3:4 mixture (by weight) of ethylene carbonate (EC), dimethyl carbonate (DMC), and ethylene methyl carbonate (EMC) by volume ratio (Technosemichem Co. Ltd, Korea) as an electrolyte in an argon-filled glove box. The cells were galvanostatically tested for (Maccor) charge and discharge cycling with current densities of 0.05 ~ 3 C and for 40 cycles (0.1 C) in the range of 2.8 ~ 4.3 V or 4.5 V to evaluate the electrochemical behavior of the cathode materials. The AC impedance (IVIUM) was measured after charges of 0.1, 0.2, 1, and 2 C for structural resistance in the range of 5 kHz to 0.1 Hz and cyclic voltammetry was conducted (CV, Macpile Biology) at a 0.05 mV/sec scan rate.

Results and Discussion

The LNCA/Pani composite was prepared to obtain composites based on the *in situ* intercalative polymerization of Pani within the mixed oxide layers. It should be noted that although this procedure was apparently successfully applied to obtain intercalation compounds of related solids such as $LiCoO_2$, $LiNiO_2$, and $LiNi_{0.8}Co_{0.2}O_2$.[20] In our case (Fig. 1), the resulting compounds consisted of a homogeneous mixture formed by Pani and the starting mixed oxide without intercalation. For the preparation of $LiNi_{0.8}Co_{0.15}Al_{0.05}O_2$/Pani composite, for aniline dispersion, the ultrasound treatment appears to be more effective than conventional methods such as magnetic stirring to produce more homogeneous material containing a large amount of metal oxide particles.

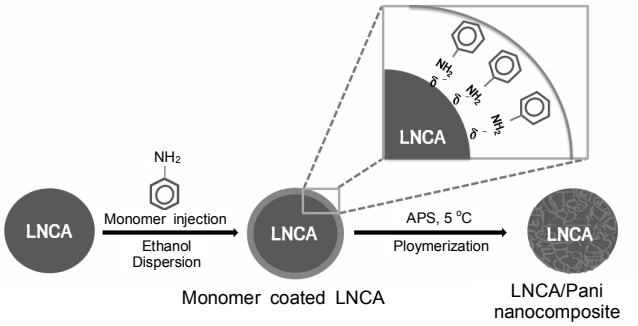

Figure 1. Preparation of LNCA/Pani composite.

FT-IR and UV-Vis spectra. Figure 2 shows FT-IR spectra of bulk Pani and the $LiNi_{0.8}Co_{0.15}Al_{0.05}O_2$/Pani composite. The adsorbance ratio of benzennoid to quinoid bands can be taken as a measure of the oxidation state in polyaniline-type conducting polymers.[21] The ratio of adsorbance of benzenoid to quinoid bands will be unity if the Pani possesses an emeraldine structure. In bulk Pani, 3,010 cm^{-1} is attributed to the N–H stretching mode and 1,477 and 1,566 cm^{-1} are

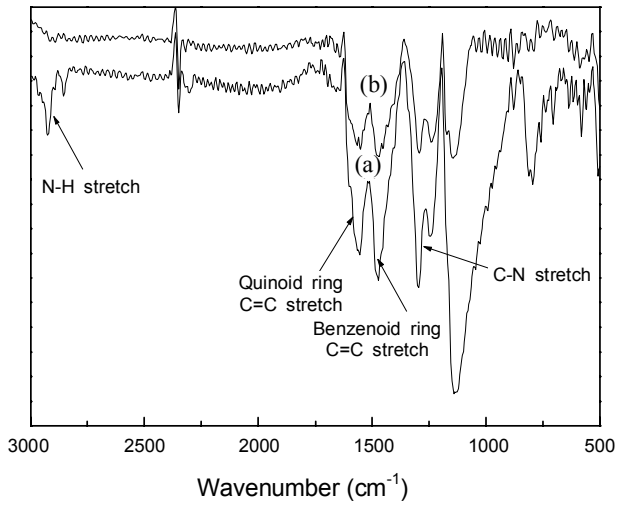

Figure 2. FT-IR spectra of (a) bulk Pani and (b) LNCA/Pani.

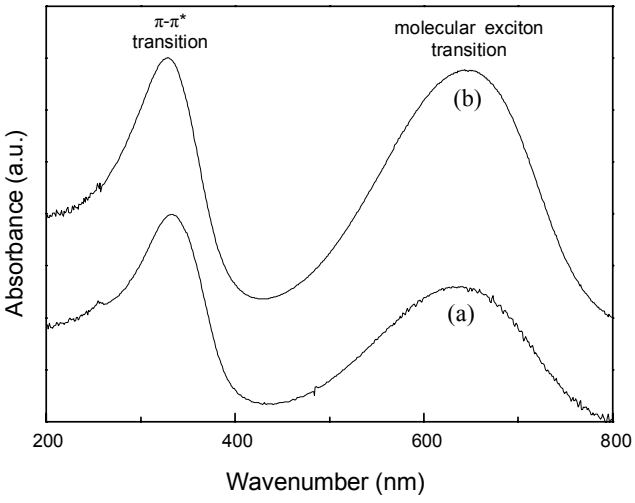

Figure 3. UV-Vis spectra of (a) bulk Pani and (b) LNCA/Pani.

attributed to the characteristic C=C stretching of the quinoid and benzenoid rings, respectively. The peaks at 1,292 and 1,245 cm^{-1} are assigned to C–N stretching modes of the benzenoid ring. The broad and strong peak at around 1,150 cm^{-1} is associated with vibrational modes of –N=quinoid=N and the peak at 772 cm^{-1} is attributed to C–H out of plane vibration. We confirmed that the peak tendencies of bulk Pani and LNCA/Pani are similar.

UV-Vis absorption spectra (Fig. 3) of bulk Pani and LNCA/Pani were recorded in NMP. For bulk Pani, two electronic bands were seen at 328 and 639 nm. These originated from the π-π* transition and benzenoid and quinoid excitonic transition respectively. For the LNCA/Pani composites, the π-π* absorption bands shifted to 310 nm. These types of shifts in the absorption bands have not been observed for composites in which metal particles are loaded onto simple LNCA in the absence of Pani.

Structural characterization. Figure 4 shows XRD patterns of the pristine LNCA and the LNCA/Pani composites. All of the diffraction patterns indicate the formation of a layered α-$NaFeO_2$ type structure assuming a hexagonal setting in the Rm space group. This convincingly demonstrates that the synthesized samples had a layered structure and did not contain another lattice. In general, the splitting degree of the hexagonal (006)/(102) and (108)/(110) as well as the intensity ratio of (003) to (104) are accepted as criteria to judge the structural ordering of materials.[22] The intensity ratio of hexagonal doublet peaks (006)/(102) to the (101) peak[23] suggests that the material has an enhanced hexagonal ordering structure. The two characteristic diffraction peaks centered correspond to Pani in its emeraldine salt form. The peak (100) reflection is slightly more intense than the peak (110) reflection. In a result, the little bit of Pani peak shows up after coating. As to the reason, Pani exists in LNCA due to coating. The average thickness of the Pani was estimated by using scherrer's equation[24]

$$D = K\lambda/\beta\cos\theta \quad (\lambda: \text{X-ray wave length } (1.5406\ \text{Å}))$$

(K: shape factor, D: average diameter of the crystals, θ: Bragg angle, β: full width at half-maximum expressed in unit of 2θ)

The Pani coating thickness is 8 ~ 9 nm. However, there was no difference between coated and uncoated particles except in the lattice parameters.

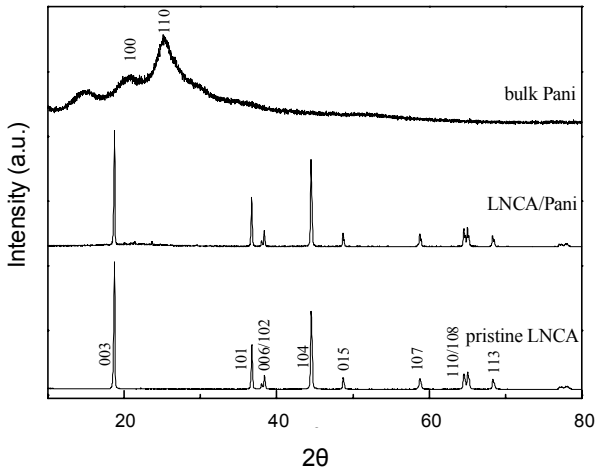

Figure 4. XRD patterns of pristine LNCA, LNCA/Pani, and bulk Pani.

Morphology. Figure 5 shows SEM micrographs of the LNCA pristine oxide and LNCA/Pani composite. The particle morphology and particle size distribution of cathode materials greatly influence battery performance. Cathode materials with small particles tend to have large initial capacity and low cycle stability and vice versa. The images show the shape and size of the electrode particles and the detailed structure of each individual particle. The LNCA sample had an average particle size of 8 ~ 10 μm with smooth particle surfaces. The pristine LNCA consisted of spherical particles. The particle size determines the effective surface area and smaller particles tend to improve the capacity of the battery by reducing the ion diffusion pathway during the insertion and desertion processes

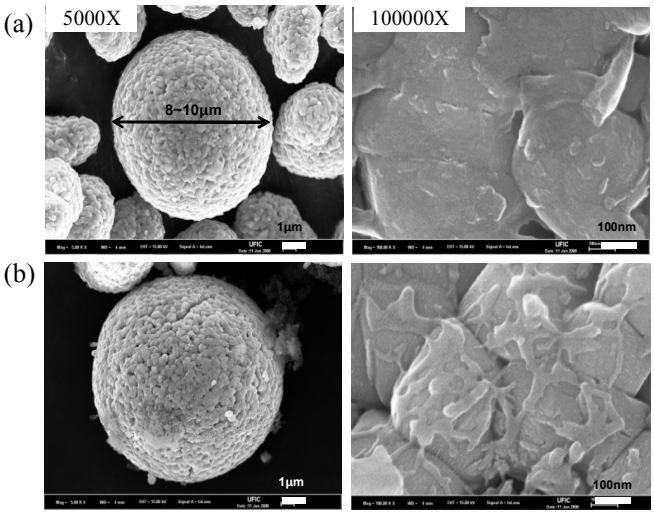

Figure 5. SEM images of (a) pristine LNCA and (b) LNCA/Pani.

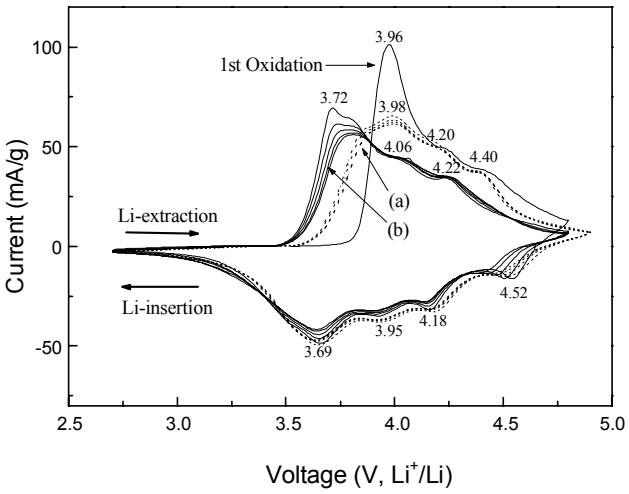

Figure 6. Cyclic voltammograms of pristine (a) LNCA and (b) LNCA/Pani with a voltage range of 2.7 ~ 4.8 V at 0.05 mV/sec.

of Li^+ ions.[25] The LNCA/Pani composite made a net form on the oxide surface so that the net form of Pani connect between the LNCA.

Electrochemical performance. Cyclic voltammetry: Cyclic voltammetry is sensitive to phase transformations of materials which occur during electrochemical reactions. Hence, slow scan cyclic voltammetry was performed to examine the effect of the coating on the phase transition that accompanies the charge-discharge processes.[26] Figure 6 shows the cyclic voltammograms of the pristine LNCA and the LNCA/Pani composite. For the pristine LNCA (Fig. 6(a)), the anodic peaks were centered at 3.98, 4.20, and 4.40 V, and correspond to delithiation from the lattice. The cathodic peaks were centered at 4.18, 3.95, and 4.52 V along with the major peak at 3.69 V, which corresponds to the intercalation of Li ions. For the coated LNCA/Pani (Fig. 6(b)), the first cycle anodic peaks were centered at 3.96, 4.20, and 4.40 V, and the cathodic peaks were the same as those seen in pristine LNCA. In the second cycle, the anodic peak was centered at a lower potential of 3.72 V. Further cycles showed minor shifts in the anodic and cathodic peak potentials, which indicate reversibility of the charge-discharge reaction. The major anodic/cathodic peaks at 3.72 V are assigned to the oxidation/reduction of Ni^{3+}/Ni^{4+} delithiation/lithiation processes. The peak potentials remained almost constant, but the relative peak intensities and area under the peak decreased with cycle number, corresponding to capacity fade. In Fig. 6(b), the minor peaks are associated with phase change. For example, the anodic peak at 3.72 V has a shoulder at ~3.78 V, which is characteristic of the two-phase region corresponding to the hexagonal (H1) to monoclinic (M) phase transition in LNCA/Pani. This peak is not evident in the cathodic peak. The anodic/cathodic peaks corresponding to 4.06/3.95 V and 4.22/4.18 V are assigned to the M to hexagonal (H2) and H2 to hexagonal (H3) phase transitions, respectively. It can be observed in Fig. 6(a) that the peaks corresponding to phase changes persisted upon continuous processing. Therefore, it is significant that coating the pristine cathode resulted in a decrease of impedance, phase transitions, and enhanced cycle stability of the materials.

AC impedance: To further investigate the improved electrochemical properties of the LNCA/Pani composites, AC impedance measurements were performed at different charge states for the LNCA and LNCA/Pani composites. Each of the impedance spectra includes two semicircles: a semicircle at high-to-medium frequencies reflecting the resistance for Li^+ ion migration through the surface film and film capacitance, and a semicircle at lower frequencies reflecting charge transfer resistance and interfacial capacitance between the electrodes

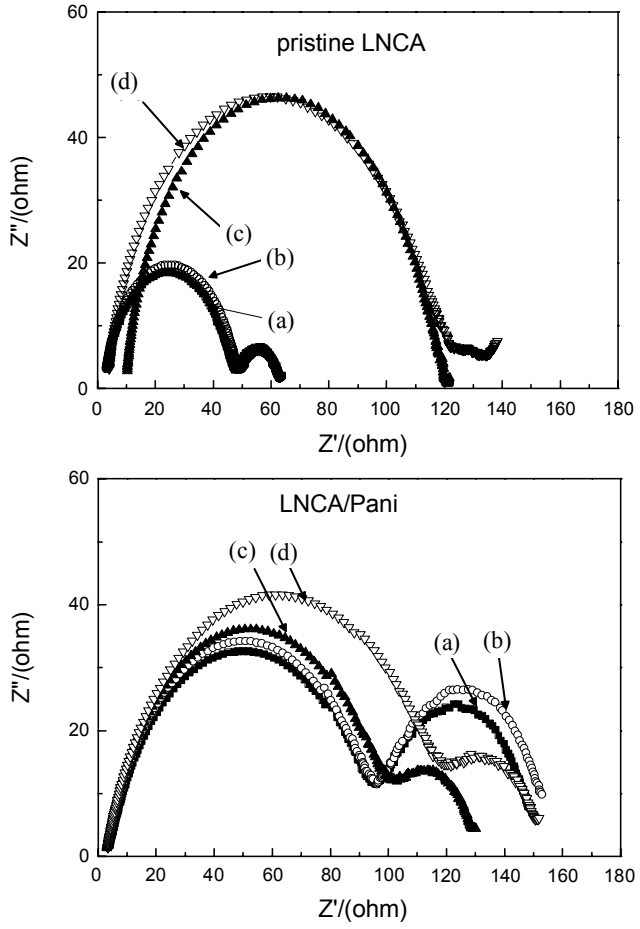

Figure 7. Nyquist plots of the cell containing pristine LNCA and LNCA/Pani charged to 2.8 ~ 4.3 V at (a) 0.1, (b) 0.2, (c) 1, and (d) 2 C.

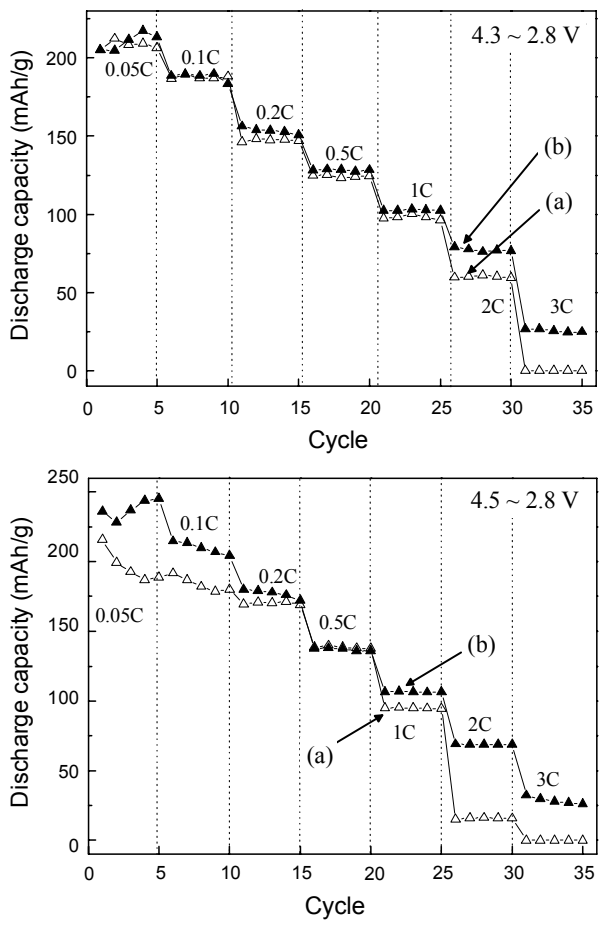

Figure 8. Discharge capacity and cyclic performance of (a) pristine LNCA and (b) LNCA/Pani with a voltage range of 4.3 and 4.5 ~ 2.8 V at 0.05, 0.1, 0.2, 1, 2, and 3 C.

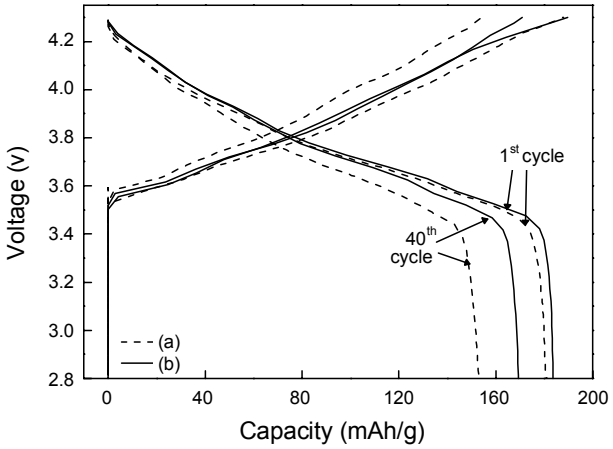

Figure 9. Charge-discharge capacities vs. cycle number of (a) pristine LNCA and (b) LNCA/Pani for 40 cycles at 0.1 C.

and electrolyte. The sloping line at very low frequencies reflects Li^+ ion diffusion in the solid state electrode. In electrochemical impedance spectroscopy of lithium-ion cells, the cell impedance is attributed mainly to cathode impedance, especially charge-transfer resistance.[27] Thus, we can obtain information about the cathode impedance change during cycling from a comparison of the first semicircle, which reflects charge-transfer resistance. It is clear from Fig. 7 that there is a pronounced difference in the second semicircle between the LNCA and LNCA/Pani composites. We investigated the effect of Pani coating about the variation of charging current for the cells by AC impedance analysis. The variation of the resistance depending on the charging current in LNCA/Pani was small than pristine LNCA. The diameter of the first semicircle of LNCA/Pani deceased from 0.1 C to 2 C and did not change at high C rates. In high C-rate (2C), the resistance of pristine LNCA and LNCA/Pani owing to the diffusion and migration of Li ions on the surface of cathode was similar, but LNCA/Pani effectively suppressed the Li+ diffusion by Pani coating layer and positively acted on the capacity retention and cycle ability.

Discharge capacity and cyclic performance: Figure 8 presents the discharge capacity and cyclic properties of the pristine LNCA and LNCA/Pani at each selected C rate at room temperature. The LNCA/Pani composite was more stable than the pristine LNCA at the high rate (2 and 3C) because the Pani coating makes a stable structure during the Li insertion-extraction reaction. In particular, at high voltage (4.5 V), the LNCA/Pani composite showed more stable rate capability at all C rates demonstrating that the synthesis of the Pani coating on the LNCA.

The cycling abilities of pristine LNCA and LNCA/Pani composites were examined *via* galvanostatic cycling test and the results are shown in Fig. 9. LNCA/Pani demonstrated the good cycling performance than pristine LNCA to 40 cycles. By coating Pani on the surface of the LNCA particles, the electrical conductivity can be significantly improved which facilitates the charge-transfer reaction, leading to better utilization of the active materials. The LNCA is embedded, thereby generating connectivity in the system by the coating. The good contact between polymer and oxide particles results in the observed increase in the electrical conductivity of the composite compared to the pristine oxide.

Conclusions

Pani was coated on LNCA particles to form LNCA/Pani composites by *in-situ* self-stabilized dispersion polymerization. By evaluating the electrochemical performance of these composites, we concluded that the Pani coating improved the electrochemical properties of LNCA and therefore facilitated the charge-transfer reaction, as confirmed by AC impedance and other electrochemical measurements. The LNCA/Pani composites show better discharge capacity and cyclabilty than the pristine LNCA at a high C rate. The LNCA/Pani had good discharge capacity and cyclability. This composite maintains the Li-insertion ability of the oxide counterpart and shows improved behavior as an electrode for rechargeable lithium batteries. Furthermore, it is possible to perform cycling at higher current values in the LNCA/Pani composite than the LNCA composite.

Acknowledgments. This work was supported by the Division of Advanced Batteries in the NGE Program (Project No. = 10016454).

References

1. Matsuhiko, N.; Satoru, Y.; Takashi, I. *Chem. Commun.***1998**, 1631.
2. Li, W.; Reimers, J. N.; Dhan, J. R. *Phys. Rev.* **1992**, *B46*, 3236.
3. Thackeray, M. M.; David, W. I. F.; Bruce, P. G. *Mater. Res. Bull.* **1983**, *18*, 461.
4. Delmas, C.; Saadoune, I.; Rougier, A. *J. Power Sources* **1993**, *43*, 595.
5. Cho, J.; Park, B. *J. Power Sources* **2001**, *92*, 359.
6. Liu, H.; Li, J.; Zhang, Z. *Electrochim. Acta* **2004**, *49*, 1151.
7. Kim, J.; Hong, Y.; Ryu, K. S. *Electrochem. Solid State Lett.* **2006**, *9*, A19.
8. Matsumoto, K.; Kuzuo, R.; Takeya, K. *J. Power Sources* **1999**, *81*, 558.
9. Chowdari, B. V. R.; Subba Rao, G. V.; Chow, S. Y. *Solid State Ionics* **2001**, *140*, 55.
10. Naghash, A. R.; Lee, J. Y. *Electrochim. Acta* **2001**, *46*, 2293.
11. Mosqueda, Y.; Perez-Cappe, E.; Arana, J. *J. Solid State Chem.* **2006**, *179*, 308.
12. Ruiz-Hitzky, E. *Adv. Mater.* **1993**, *5*, 334.
13. Gomez-Romeo, P. *Adv. Mater.* **2001**, *13*, 163.
14. Tang, B. Z.; Geng, Y.; Lam, J. W. Y. *Chem. Mater.* **1999**, *11*, 1581.
15. Yoneyama, H.; Kuwabata, S. *J. Chem. Soc. Chem. Commun.* **1991**, 986.
16. Kuwabata, S.; Masui, S.; Tomiyori, H. *Electrochim. Acta* **2000**, *46*, 91.
17. MacDiarmid, A. G. Angew. *Chem. Int. Ed.* **2001**, *40*, 2581.
18. Pei, Q.; Yu, G.; Zhang, C. *Science* **1995**, *269*, 1086.
19. Cao, Y.; Smith, P.; Heeger, A. G. *US. Pat.* **1993**, 5232631.
20. Ramachandran, K.; Christopher, O.; Lerner, M. *Mater. Res. Bull.* **1996**, *31*, 767.
21. Prevost, V.; Petit, A.; Pla, F. *Synth. Met.* **1999**, *104*, 79.
22. Ohuzuku, T.; Ueda, A.; Nagayama, M. *J. Electrochem. Soc.* **1993**, *140*, 1862.
23. Reimers, J. N.; Rosen, E.; Jones, C. D. *Solid State Ionics* **1993**, *61*, 335.
24. Klong, H. P.; Alexander, L. E. *X-ray Diffraction Procedures for Crystalline and Amorphous Materials*; Wiley: New York, 1954.
25. Cho, J.; Park, B. *J. Power Sources* **2001**, *92*, 35.
26. Kavan, L.; Gratzel, M. *Electrochem. Solid State Lett.* **2002**, *5*, A39.
27. Chen, C. H.; Liu, J.; Amine, K. *J. Power Sources* **2001**, *96*, 321.